 Printed in China Communications in Theoretical Physics

Commun. Theor. Phys. **77** (2025) 035702 (6pp) https://doi.org/10.1088/1572-9494/ad8db7

Interacting bosons on a four-leg flux ladder

Dian-Cheng Zhang[1,*] **and Shi-Jie Yang**[2]

[1] College of Science, Hainan Tropical Ocean University, Sanya, Hainan 572022, China
[2] Department of Physics, Beijing Normal University, Beijing 100875, China

E-mail: zhangdiancheng16@mails.ucas.ac.cn

Received 28 May 2024, revised 10 October 2024
Accepted for publication 31 October 2024
Published 13 December 2024

Abstract

We conduct a dynamical Gutzwiller mean-field study of interacting bosons on a four-leg ladder, subject to a uniform flux. The ground states dependent on the magnetic flux and kinetic tunneling strength are explored. Consequently, we identify the super-vortical lattice, as well as the inner-Meissner phase, which presents Meissner currents just along the intimal legs within the flux ladder. The staggered-current phase is also allowed, with its formation condition altered because of the four-leg construction. The number of legs on the flux ladder can make an effect.

Keywords: interacting bosons, flux ladder, Meissner phase, vortical lattice

(Some figures may appear in colour only in the online journal)

1. Introduction

Due to these highly controllable and flexible properties, ultracold atoms loaded in the optical lattice establish an elegant platform for emulating many-body physics of intricate solid-state systems [1–3], with a clean and well-controlled circumstance. Regarding the bosonic lattice, its abundant unusual states could be described by the celebrated Bose–Hubbard (BH) model [4–6], from which one can illustrate the typical superfluid (SF) state, as well as an incompressible Mott insulating (MI) state [7]. In particular, alternating densities can be observed within the density-wave (DW) and supersolid (SS) regimes [8–10], subject to the long-range interaction. Another promising route in the quest for nontrivial quantum phases is to introduce an external magnetic field on the lattice system [11–13]. It is expected to break the time reversal symmetry of systems. Increasingly experimental implementations of complex artificial gauge fields have made striking progress in recent years [14–17].

Among the diverse optical lattices of chosen geometries, the one dimensional (1D) optical lattice has attracted a wealth of extraordinary explorations in the past two decades. Exposed to a uniform or a staggered magnetic flux, it is primarily created as the 'ladder', whose number of legs is far less than that of rungs in a finite system. Abundant quantum behaviors emanate from flux ladders, with the Meissner current serving as a prominent example [18], which presents an ascendant analogue of its counterpart caused by the substantive superconductivity. Since the Meissner phase on the lattice was originally formulated [18], it has inspired theoretical works that propose multiple intriguing phenomena dependent of flux ladders, such as the vortical lattice (VL) featuring chiral vortical currents [19–21], the chiral MI state [22–24], Laughlin states connected to the Fractional Hall effect [25–28], the biased ladder (BL) phase showing an imbalance of densities between two legs [29–32], as well as the Hofstadter butterfly [33–35]. Experimentally, a compelling realization of the Meissner currents is reported [36]. It has been further generated in a Fock space [37]. During the last few years, there are also flourishing proposals about the novel Peierls phase [38–41].

Confined in one 1D lattice, the usually adopted numerical method is known as the density matrix renormalization group (DMRG) [42–44], which works effectively with a high precision. Even so, when the lattice's width (the number of legs) is considerably enlarged, the validity of the DMRG arguably becomes attenuate [45]. In addition, previous efforts on flux ladders pay more attention to lattices comprised of no more than three legs [30, 46, 47]. Potential structures of ground states residing on four-leg bosonic ladders, or ladders consisting of more legs come to be interesting themes, and deserve more attempts on attendant schemes.

In this manuscript, we choose a four-leg bosonic lattice as the target, subject to a uniform magnetic field. Spectacular performances of this system would be figured out by employing the dynamical Gutzwiller mean-field theory (DGMFT) [48–50], whose substantial advantage is to feasibly solve a ladder model composed of a great amount of legs, and map out ground states

* Author to whom any correspondence should be addressed.

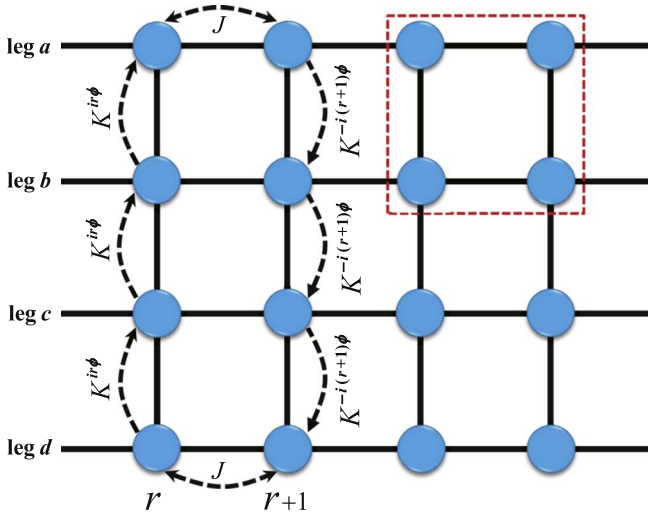

Figure 1. The schematic diagram of the four-leg ladder lattice subject to an external and uniform magnetic flux. From the top to bottom, *a*, *b*, *c*, and *d* indicate those four different legs respectively. The tunneling amplitude J only works horizontally on the inner leg, while the inter-leg complex hopping element contributes to a phase factor ϕ, with K corresponding to the strength of tunneling. The red dashed box surrounds one plaquette which consists of four sites.

site by site. The resulting numerical solutions are worth mentioning due to their appealing structures, including the inner-Meissner phase, the super-vortical lattice, as well as the staggered-current phase. We further probe the model consisting of five legs. Consequently, the quantum phases experience an alteration, meaning that the number of legs could make an impact on the ground states of the flux ladder.

The remainder of this paper is structured as follows: in section 2, we outline the BH model entailing the artificial magnetic flux, and the method used, followed by a presentation of results and discussion in section 3. A brief summary is given by section 4.

2. Model and method

The bosonic flux ladder consisting of four legs is concisely sketched in figure 1, whose Hamilton is described by the BH model, taking the form as below:

$$\hat{H} = \sum_{r,\sigma}\left[\frac{U}{2}\hat{n}_r^{\sigma}(\hat{n}_r^{\sigma}-1)-\mu\hat{n}_r^{\sigma}\right] - J\sum_{r,\sigma}(\hat{\sigma}_r^{\dagger}\hat{\sigma}_{r+1}+h.c.) - K\sum_{r}(\hat{a}_r^{\dagger}\hat{b}_r e^{-ir\phi}+\hat{b}_r^{\dagger}\hat{c}_r e^{-ir\phi}+\hat{c}_r^{\dagger}\hat{d}_r e^{-ir\phi}+h.c.), \tag{1}$$

where the four different legs are labeled by $\sigma = a, b, c, d$ respectively, with r symbolizing the index of the rung. J is the tunneling amplitude on the inner leg, and K represents the tunneling amplitude between two neighboring legs, but along the rung. $\hat{\sigma}_r^{\dagger}(\hat{\sigma}_r)$ creates (annihilates) a boson on leg σ and the rth rung, while $\hat{n}_r^{\sigma}$ refers to the relevant particle number operator. The phase factor ϕ describes an artificial flux quantum applied on each plaquette. μ is the chemical potential, and U corresponds to the on-site interaction. For simplicity, a constant $U = 1$ is chosen in this paper.

To figure out the ground states of the system, we take advantage of the DGMFT, whose foundation is on the Gutzwiller variational wavefunction, which can be written as follows

$$|\Psi\rangle = \prod_{\sigma,r}\sum_{N=0}^{N_{\max}} f_N^{(\sigma,r)}\ |N\rangle_{\sigma,r}. \tag{2}$$

Here, $|N\rangle_{\sigma,r}$ refers to the local Fock basis on one site, whose lattice indices belong to the rth rung and leg σ. An invariant $N_{\max} = 6$ is exploited in this context, as a truncation of the local maximum occupancy per site. $f_N^{(\sigma,r)}$ are complex coefficients, which should satisfy the normalization condition

$$\sum_{N=0}^{N_{\max}} |f_N^{(\sigma,r)}|^2 = 1. \tag{3}$$

The mean-field decoupling approximation would give

$$\hat{\sigma}_r^{\dagger}\hat{\sigma}_{r+1} = \varphi_{\sigma,r}^{*}\hat{\sigma}_{r+1} + \hat{\sigma}_r^{\dagger}\varphi_{\sigma,r+1} - \varphi_{\sigma,r}^{*}\varphi_{\sigma,r+1}. \tag{4}$$

Here the SF order parameters with respect to four legs are determined by

$$\varphi_{\sigma,r} = \langle\hat{\sigma}_r\rangle = \langle\Psi|\hat{\sigma}_r|\Psi\rangle = \sum_N \sqrt{N+1}\,[f_N^{(\sigma,r)}]^{*} f_{N+1}^{(\sigma,r)}. \tag{5}$$

Similarly, the occupancy of each site reads

$$n_{\sigma,r} = \langle\hat{n}_r^{\sigma}\rangle = \langle\Psi|\hat{n}_r^{\sigma}|\Psi\rangle = \sum_N N\,|f_N^{(\sigma,r)}|^2. \tag{6}$$

Considering all the above ansatzes, and substituting the Gutzwiller wavefunction into that time-dependent Schrodinger equation, one can eventually obtain four evolving equations about $f_N^{(\sigma,r)}$ [48–50]. They could be further written as

$$\begin{aligned}
i\hbar\partial_t f_N^{(a,r)} =& [Un_{a,r}(n_{a,r}-1)/2-\mu n_{a,r}]f_N^{(a,r)} \\
&- K\varphi_{b,r}^{*}e^{ir\phi}\sqrt{N+1}f_{N+1}^{(a,r)} \\
&- [J(\varphi_{a,r-1}+\varphi_{a,r+1}) \\
&+ K\varphi_{b,r}e^{-ir\phi}]\sqrt{N}f_{N-1}^{(a,r)}, \\
i\hbar\partial_t f_N^{(b,r)} =& -[J(\varphi_{b,r-1}^{*}+\varphi_{b,r+1}^{*}) \\
&+ K(\varphi_{a,r}^{*}e^{-ir\phi}+\varphi_{c,r}^{*}e^{ir\phi})]\sqrt{N+1}f_{N+1}^{(b,r)} \\
&- [J(\varphi_{b,r-1}+\varphi_{b,r+1})+K(\varphi_{a,r}e^{ir\phi} \\
&+ \varphi_{c,r}e^{-ir\phi})]\sqrt{N}f_{N-1}^{(b,r)} \\
&+ [Un_{b,r}(n_{b,r}-1)/2-\mu n_{b,r}]f_N^{(b,r)}, \\
i\hbar\partial_t f_N^{(c,r)} =& -[J(\varphi_{c,r-1}^{*}+\varphi_{c,r+1}^{*}) \\
&+ K(\varphi_{b,r}^{*}e^{-ir\phi}+\varphi_{d,r}^{*}e^{ir\phi})]\sqrt{N+1}f_{N+1}^{(c,r)} \\
&- [J(\varphi_{c,r-1}+\varphi_{c,r+1})+K(\varphi_{b,r}e^{ir\phi} \\
&+ \varphi_{d,r}e^{-ir\phi})]\sqrt{N}f_{N-1}^{(c,r)} \\
&+ [Un_{c,r}(n_{c,r}-1)/2-\mu n_{c,r}]f_N^{(c,r)}, \\
i\hbar\partial_t f_N^{(d,r)} =& [Un_{d,r}(n_{d,r}-1)/2-\mu n_{d,r}]f_N^{(d,r)} \\
&- K\varphi_{c,r}^{*}e^{-ir\phi}\sqrt{N+1}f_{N+1}^{(d,r)} \\
&- [J(\varphi_{d,r-1}+\varphi_{d,r+1}) \\
&+ K\varphi_{c,r}e^{ir\phi}]\sqrt{N}f_{N-1}^{(d,r)}.
\end{aligned} \tag{7}$$

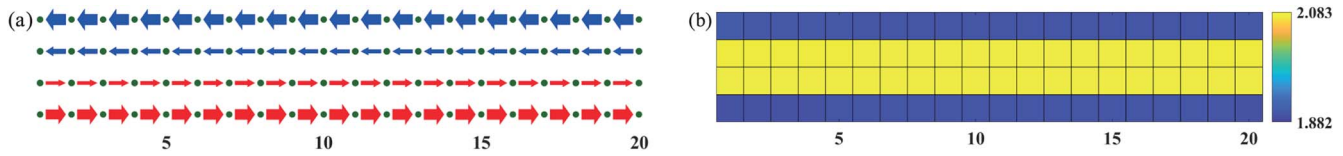

Figure 2. The ground state corresponding to $\mu = 1$, $J = 0.2$, $K = 0.2$, and $\phi = \pi/10$. (a) describes the particle currents. The red arrows denote positive currents from the rth to the $(r+1)$ th rung, while the blue arrows mark those reverse-direction currents. The thickness of these arrows encodes the strength of local currents. (b) describes local occupancies, with the colorbar indicates the magnitude of the occupancy.

Equation (7) is a nonlinear equation, which can be solved self-consistently under the two equations (5) and (6) via the standard imaginary-time-evolution technique.

In our calculation, the length of the ladder lattice is determined by $L = 80$, with the periodic boundary condition. According to previous works [30, 47], the longitudinal current operators along legs are given by

$$j^{\parallel}_{r,\sigma} = -\mathrm{i}J(\hat{\sigma}^{\dagger}_{r+1}\hat{\sigma}_r - \hat{\sigma}^{\dagger}_r\hat{\sigma}_{r+1}), \tag{8}$$

while those vertical current operator perpendicular to the leg read

$$\begin{aligned} j^{\perp}_{r,ab} &= -\mathrm{i}K(\mathrm{e}^{-\mathrm{i}r\phi}\hat{a}^{\dagger}_r\hat{b}_r - \mathrm{e}^{\mathrm{i}r\phi}\hat{b}^{\dagger}_r\hat{a}_r), \\ j^{\perp}_{r,bc} &= -\mathrm{i}K(\mathrm{e}^{-\mathrm{i}r\phi}\hat{b}^{\dagger}_r\hat{c}_r - \mathrm{e}^{\mathrm{i}r\phi}\hat{c}^{\dagger}_r\hat{b}_r), \\ j^{\perp}_{r,cd} &= -\mathrm{i}K(\mathrm{e}^{-\mathrm{i}r\phi}\hat{c}^{\dagger}_r\hat{d}_r - \mathrm{e}^{\mathrm{i}r\phi}\hat{d}^{\dagger}_r\hat{c}_r). \end{aligned} \tag{9}$$

3. Numerical results

In our protocol, only the first twenty rungs are displayed for clarity. Throughout this manuscript, the chemical potential and intra-leg tunneling amplitude are fixed as $\mu = 1$, and $J = 0.2$. We begin with a small magnetic flux $\phi = \pi/10$, and $K = J$. The resulting structure of the ground state is mapped out in figure 2. Its local currents are comprised of two distinct constituents, one of which is the leftward current along leg a and b, labeled by the blue arrow in figure 2(a). The other is oriented horizontally towards the right side, and marked by the red arrow on leg c, as well as leg d. And as a consequence, a collection of local currents on leg b and leg c develop the Meissner current, just sandwiched inside the four-leg bosonic ladder. It is named the inner-Meissner phase hereafter. Additionally, figure 2(b) describes relevant occupancies site by site. As observed, both leg b and c capture higher particle populations than those of leg a and d. This particular imbalance of occupancies implies an underlying physical mechanism behind the inner-Meissner currents.

As predicted in earlier investigations, an enlarged flux would contribute to a VL state [19–21]. In what follows, we would like to increase the flux quanta. For instance, figure 3 corresponds to $\phi = \pi/2$. In figure 3(a) where $J = 0.2$, and $K/J = 0.2$, the structure of the ground state is characterized by a number of supercells, some of which are schematically encircled by dashed black rectangular boxes. Inside one certain supercell, three chiral vortical particle currents emerge, and each of them occupies one plaquette. Though a modulated density distribution exhibited in the right column, local currents bridging two adjacent supercells capture no chiral properties. Figure 3(b) is connected with $K/J = 0.1$, and there are also a range of vortexes, with every two neighboring ones featuring opposite orientations. As each vortex encompasses six plaquettes in total, we prefer to call it the 'super-vortical lattice' (SVL) state, distinguished from the VL state generated by a flux ladder possessing less than four legs. Intriguingly, as observed in the right column of figure 3(b), within a single supercell, it presents larger occupancies on the two inner sites, than those on the marginal sites. Moreover, when the flux quantum is close to π, just like $\phi = 4\pi/5$ in figure 3(c), the construction of the SVL state varies. Concretely speaking, the configuration of figure 3(c) is filled with two categories of vortexes. One is the small vortex which vertically embraces three plaquettes, and the other behaves as a big vortex containing six plaquettes on the whole. Three consecutive small vortexes followed by a big vortex actually build up an alternating sequence, in coincidence with which the distribution of occupancies goes through an analogical arrangement.

When an enhanced flux quanta locates in the vicinity of π, the staggered-current (SC) phase comes into sight, as displayed by figure 4, whose physical parameters are chosen as $\phi = 15\pi/16$, $J = 0.2$, and $K/J = 2$. Though the SC phase has been reported in a three-leg flux ladder [47], compared with which, there are two different types of rectangular vortexes presented in figure 4(a). As observed, the first type involves a single plaquette per vortex, and each of the second category entails two plaquettes on the whole. Meanwhile, during the transformation from the former type to the latter one, the relevant distribution of occupancies also undergoes a discrepancy, which could be commodiously found out from figure 4(b). The clockwise and counterclockwise orientations are respectively captured by every two neighboring vortexes. Nonetheless, in our calculation, with an enormous flux quanta approaching π, these chiral vortexes of a SC state could not be further discovered in the scenery where $K \leqslant J$. This restriction is not necessary for that SC state in [47], which is derived from a flux ladder consisting of three legs.

Up to now, the above discussions basically focus on the four-leg ladder lattice, subject to a uniform magnetic flux. Just as aforementioned, one could generalize the BH model to a flux lattice which is comprised of more than four chains. Figure 5 exemplifies fascinating behaviors of local currents on a five-leg flux ladder. For $\phi = \pi/2$, the SVL state could be successfully reproduced at $J = 0.2$, and $K/J = 0.1$, as depicted by figure 5(a), whose physical parameters are identical to those

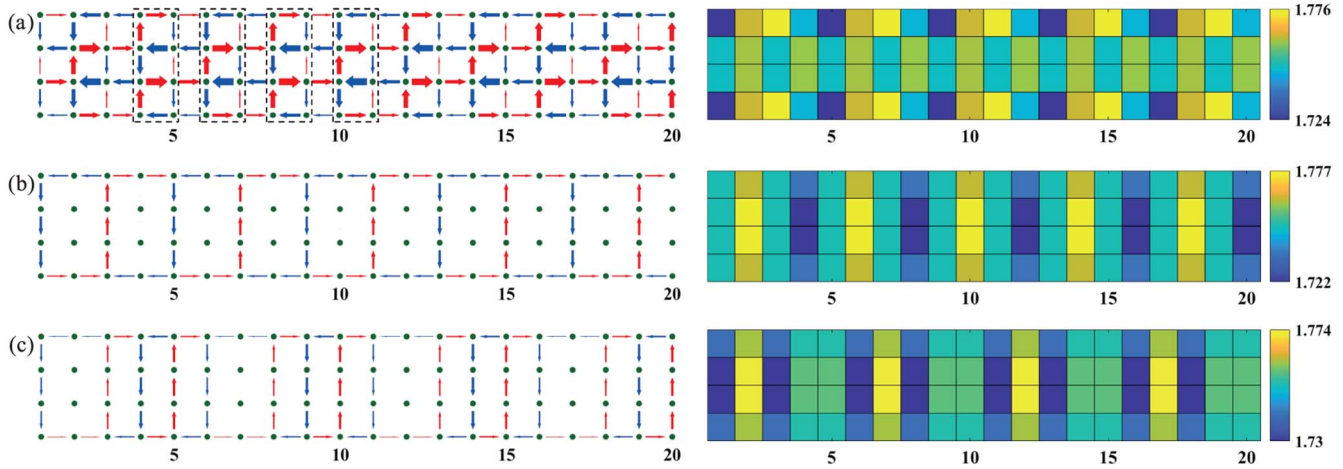

Figure 3. The ground states corresponding to $\mu = 1$, and $J = 0.2$. From the top to bottom, (a) is related to $K = 0.04$, and $\phi = \pi/2$; (b) is related to $K = 0.02$, and $\phi = \pi/2$; (c) is related to $K = 0.02$, and $\phi = 4\pi/5$. The left column describes local particle currents, and the right column describes relevant occupancies.

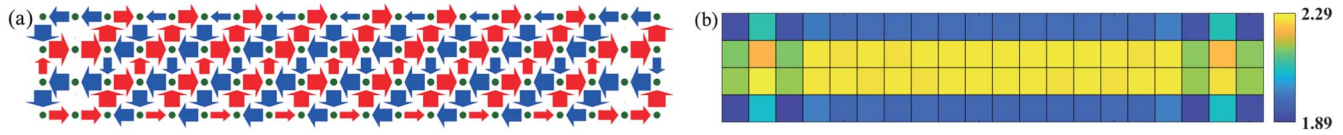

Figure 4. The ground state corresponding to $\mu = 1$, $J = 0.2$, $K = 0.4$, and $\phi = 15\pi/16$. (a) describes the particle currents, and (b) describes relevant occupancies.

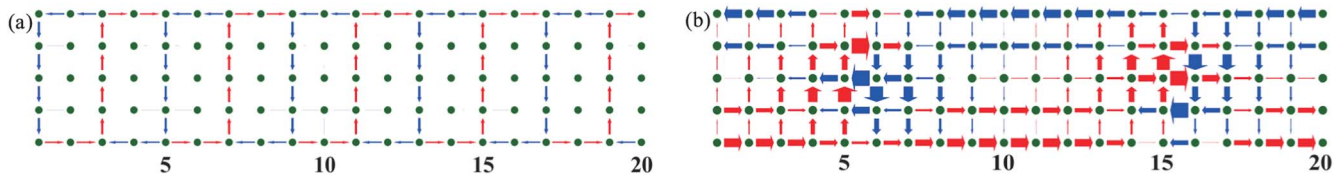

Figure 5. The particle currents of the flux ladder comprised of five legs, related to $\mu = 1$, and $J = 0.2$. (a) corresponds to $K = 0.02$, and $\phi = \pi/2$; (b) corresponds to $K = 0.2$, and $\phi = \pi/10$.

Table 1. Classification of quantum phases supported by the flux ϕ and the value of K/J.

Quantum phase	Physical parameter
inner-Meissner	$0 < \phi \leqslant \pi/10$, $K/J \geqslant 1$
super-vortical lattice	$\pi/2 \leqslant \phi \leqslant 7\pi/8$, $0 < K/J \leqslant 0.1$
staggered-current	$7\pi/8 < \phi < \pi$, $K/J > 1$

of figure 3(b). Similarly, the physical parameters in figure 5(b) are consistent with those in figure 2. However, the ground state in figure 5(b) presents non-zero vertical currents as well as longitudinal ingredients, instead of inner-Meissner currents in figure 2. In other words, the increasing number of legs puts an influence on the ground state of a ladder in the presence of a small flux. Furthermore, the SC state associated with a big flux, and classically illustrated in figure 4, also fails to experience a recurrence depending on a five-leg ladder. In our numerical simulation, it manifests that ground states derived from $\phi = \pi/2$ are not susceptible to the growth of the amount of legs. We further list appropriate parameters corresponding to different quantum phases, described in table 1.

4. Summary

We investigate the quantum phases of interacting ultracold bosons loaded in a four-leg ladder lattice, which is subject to a uniform artificial gauge field. By employing a dynamical Gutzwiller mean-field theory, we figure out the ground states of the system site by site. As a consequence, the inner-Meissner current only along the central legs within the flux ladder is discovered. We further identify a super-vortical lattice state, apart from the staggered-current phase. Finally, the influence of the number of legs on the ground state is shortly discussed, based on the BH model of flux ladder.

Acknowledgments

This work is supported by the Scientific Research Foundation of Hainan Tropical Ocean University (Grant No. RHDRC202301).

References

[1] Trefzger C, Menotti C, Capogrosso-Sansone B and Lewenstein M 2011 Ultracold dipolar gases in optical lattices *J. Phys.* B **44** 193001
[2] Eckardt A 2017 Colloquium: atomic quantum gases in periodically driven optical lattices *Rev. Mod. Phys.* **89** 011004
[3] Schafer F, Fukuhara T, Sugawa S, Takasu Y and Takahashi Y 2020 Tools for quantum simulation with ultracold atoms in optical lattices *Nat. Rev. Phys.* **2** 411
[4] Jaksch D, Bruder C, Cirac J I, Gardiner C W and Zoller P 1998 Cold bosonic atoms in optical lattices *Phys. Rev. Lett.* **81** 3108
[5] Cazalilla M A, Citro R, Giamarchi T, Orignac E and Rigol M 2011 One dimensional bosons: from condensed matter systems to ultracold gases *Rev. Mod. Phys.* **83** 1405
[6] Dutta O, Gajda M, Hauke P, Lewenstein M, Luhmann D-S, Malomed B A, Sowinski T and Zakrzewski J 2015 Non-standard Hubbard models in optical lattices: a review *Rep. Prog. Phys.* **78** 066001
[7] Greiner M, Mandel O, Esslinger T, Hansch T W and Bloch I 2002 Quantum phase transition from a superfluid to a Mott insulator in a gas of ultracold atoms *Nature* **415** 39
[8] Leonard J, Morales A, Zupancic P, Esslinger T and Donner T 2017 Supersolid formation in a quantum gas breaking a continuous translational symmetry *Nature* **543** 87
[9] Li J R, Lee J, Huang W, Burchesky S, Shteynas B, Top F C, Jamison A O and Ketterle W 2017 A stripe phase with supersolid properties in spin-orbit-coupled Bose–Einstein condensates *Nature* **543** 91
[10] Chen H J, Yu Y Q, Zheng D C and Liao R Y 2020 Extended Bose–Hubbard model with cavity-mediated infinite-range interactions at finite temperatures *Sci. Rep.* **10** 9076
[11] Dalibard J, Gerbier F, Juzeliunas G and Ohberg P 2011 Colloquium: artificial gauge potentials for neutral atoms *Rev. Mod. Phys.* **83** 1523
[12] Roscilde T 2014 Thermometry of cold atoms in optical lattices via artificial gauge fields *Phys. Rev. Lett.* **112** 110403
[13] Goldman N, Juzeliunas G, Ohberg P and Spielman I B 2014 Light-induced gauge fields for ultracold atoms *Rep. Prog. Phys.* **77** 126401
[14] Spielman I B 2009 Raman processes and effective gauge potentials *Phys. Rev.* A **79** 063613
[15] Lin Y J, Jimenez-Garcia K and Spielman I B 2011 Spin-orbit-coupled Bose–Einstein condensates *Nature* **471** 83
[16] Wu Z, Zhang L, Sun W, Xu X T, Wang B Z, Ji S C and Deng Y 2016 Realization of two-dimensional spin-orbit coupling for Bose–Einstein condensates *Science* **354** 83
[17] Wang Z Y *et al* 2021 Realization of an ideal Weyl semimetal band in a quantum gas with 3D spin-orbit coupling *Science* **372** 271
[18] Orignac E and Giamarchi T 2001 Meissner effect in a bosonic ladder *Phys. Rev.* B **64** 144515
[19] DiDio M, DePalo S, Orignac E, Citro R and Chiofalo M L 2015 Persisting Meissner state and incommensurate phases of hard-core boson ladders in a flux *Phys. Rev.* B **92** 060506(R)
[20] Orignac E, Citro R, Dio M D, Palo S D and Chiofalo M L 2016 Incommensurate phases of a bosonic two-leg ladder under a flux *New. J. Phys.* **18** 055017
[21] Barbarino S, Sangiovanni G and Budich J C 2019 First-order topological quantum phase transition in a strongly correlated ladder *Phys. Rev.* B **99** 075158
[22] Dhar A, Maji M, Mishra T, Pai R V, Mukerjee S and Paramekanti A 2012 Bose–Hubbard model in a strong effective magnetic field: Emergence of a chiral Mott insulator ground state *Phys. Rev.* A **85** 041602(R)
[23] Dhar A, Mishra T, Maji M, Pai R V, Mukerjee S and Paramekanti A 2013 Chiral Mott insulator with staggered loop currents in the fully frustrated Bose–Hubbard model *Phys. Rev.* B **87** 174501
[24] Romen C and Lauchli A 2018 Chiral Mott insulators in frustrated Bose–Hubbard models on ladders and two-dimensional lattices: a combined perturbative and density matrix renormalization group study *Phys. Rev.* B **98** 054519
[25] Grusdt F and Honing M 2014 Realization of fractional Chern insulators in the thin-torus limit with ultracold bosons *Phys. Rev.* A **90** 053623
[26] Strinati M C, Cornfeld E, Rossini D, Barbarino S, Dalmonte M, Fazio R, Sela E and Mazza L 2017 Laughlin-like states in bosonic and fermionic atomic synthetic ladders *Phys. Rev.* X **7** 021033
[27] Petrescu A, Piraud M, Roux G, McCulloch I P and LeHur K 2017 Precursor of the Laughlin state of hard-core bosons on a two-leg ladder *Phys. Rev.* B **96** 014524
[28] Strinati M C, Sahoo S, Shtengel K and Sela E 2019 Pretopological fractional excitations in the two-leg flux ladder *Phys. Rev.* B **99** 245101
[29] Wei R and Mueller E J 2014 Theory of bosons in two-leg ladders with large magnetic fields *Phys. Rev.* A **89** 063617
[30] Greschner S, Piraud M, Heidrich-Meisner F, McCulloch I P, Schollwock U and Vekua T 2015 Spontaneous increase of magnetic flux and chiral-current reversal in bosonic ladders: swimming against the tide *Phys. Rev. Lett.* **115** 190402
[31] Barbarino S, Taddia L, Rossini D, Mazza L and Fazio R 2015 Magnetic crystals and helical liquids in alkaline-earth fermionic gases *Nat. Commun.* **6** 8134
[32] Uchino S 2016 Analytical approach to a bosonic ladder subject to a magnetic field *Phys. Rev.* A **93** 053629
[33] Hugel D, Strand H U R, Werner P and Pollet L 2017 Anisotropic Harper–Hofstadter–Mott model: competition between condensation and magnetic fields *Phys. Rev.* B **96** 054431
[34] Chen J D, Tu H H, Wu Y H and Xu Z F 2020 Quantum phases of two-component bosons on the Harper–Hofstadter ladder *Phys. Rev.* A **102** 043322
[35] Johnstone D, Ohberg P and Duncan C W 2023 Interacting bosons on crystalline and quasiperiodic ladders in a magnetic field *Phys. Rev. Research.* **5** 023195
[36] Atala M, Aidelsburger M, Lohse M, Barreiro J T, Paredes B and Bloch I 2014 Observation of chiral currents with ultracold atoms in bosonic ladders *Nat. Phys.* **10** 588
[37] Mumford J 2022 Meissner effect in Fock space *Phys. Rev.* A **106** 043325
[38] Gonzalez-Cuadra D, Grzybowski P R, Dauphin A and Lewenstein M 2018 Strongly correlated bosons on a dynamical lattice *Phys. Rev. Lett.* **121** 090402
[39] Wang B, Dong X Y, Unal F N and Eckardt A 2021 Robust and ultrafast state preparation by ramping artificial gauge potentials *New. J. Phys.* **23** 063017
[40] Chanda T, Gonzalez-Cuadra D, Lewenstein M, Tagliacozzo L and Zakrzewski J 2022 Devil's staircase of topological Peierls insulators and Peierls supersolids *SciPost Phys.* **12** 076
[41] Bacciconi Z, Andolina G, Chanda T, Chiriaco G, Schiro M and Dalmonte M 2023 First-order photon condensation in magnetic cavities: a two-leg ladder model *SciPost Phys.* **15** 113
[42] White S R 1992 Density matrix formulation for quantum renormalization groups *Phys. Rev. Lett.* **69** 2863

[43] Niyaz P, Scalettar R T, Pong C Y and Batrouni G G 1994 Phase transitions in an interacting boson model with near-neighbor repulsion *Phys. Rev.* B **50** 362
[44] Kuhner T D and Monien H 1998 Phases of the one-dimensional Bose–Hubbard model *Phys. Rev.* B **58** R14741
[45] Schollwock U 2005 The density-matrix renormalization group *Rev. Mod. Phys.* **77** 259
[46] Urba L, Lundh E and Rosengren A 2006 One-dimensional extended Bose–Hubbard model with a confining potential: a DMRG analysis *J. Phys. B: At. Mol. Opt. Phys.* **39** 5187
[47] Kolley F, Piraud M, McCulloch I P, Schollwock U and Heidrich-Meisner F 2015 Strongly interacting bosons on a three-leg ladder in the presence of a homogeneous flux *New. J. Phys.* **17** 092001
[48] Jaksch D, Venturi V, Cirsac J I, Williams C J and Zoller P 2002 Creation of a molecular condensate by dynamically melting a mott insulator *Phys. Rev. Lett.* **89** 040402
[49] Kovrizhin D L, Pai G V and Sinha S 2005 Density wave and supersolid phases of correlated bosons in an optical lattice *Europhys. Lett.* **72** 162
[50] Mazzarella G, Giampaolo S M and Illuminati F 2006 Extended Bose Hubbard model of interacting bosonic atoms in optical lattices: from superfluidity to density waves *Phys. Rev.* A **73** 013625